processes

MDPI

Article

Study on the Disintegration Resistance of Different Types of Schist on the Eastern Slope of the Tongman Open-Pit Mine

Yiming Wen [1,2], Xiangdong Niu [1,2,*], Yongfeng Lu [1,2], Yong Cheng [1,2], Ping Lu [2], Jianbo Xia [2], You Lin [2], Li Tang [2], Qi Nie [2] and Kaishan Lin [2]

[1] Faculty of Metallurgy and Mining Engineering, Kunming Metallurgy College, Kunming 650033, China; yimingwen-kmmc@foxmail.com (Y.W.); m15587023915@163.com (Y.L.)
[2] School of Land and Resources Engineering, Kunming University of Science and Technology, Kunming 650093, China
* Correspondence: niuxiangdong@stu.kust.edu.cn; Tel.: +86-15198934646

Abstract: This study aimed to investigate the disintegration resistance of schist on the eastern slope of the Tongman open-pit mine. It examined the effects of cycle number and mineral composition on the disintegration resistance indexes of four types of schist through thin section identification and laboratory disintegration resistance tests. Furthermore, we analyzed the morphological characteristics of the disintegration residues using laboratory tests. Based on pore micro-damage theory, the mechanisms responsible for the differences in disintegration resistance among the four types of schist were further explored. The results show a negative correlation between the disintegration resistance index and the number of cycles. For the same number of cycles, the disintegration resistance indices for the four schist types were ranked as follows: greenish-gray chlorite-bearing muscovite schist > gray weakly chloritized biotite–muscovite schist > greenish-gray muscovite schist > gray muscovite schist. The disintegration residues of schist samples were categorized into four morphological patterns: thin sheet-like, moderately thick sheet-like, blocky, and granular. These patterns were then thoroughly elucidated. The differences in the disintegration resistance characteristics of schist were closely related to their material composition. The microstructural pore damage within the rock is the essential factor causing schist disintegration. Variations in rock porosity led to differing damage factors, which explain the distinct disintegration resistance characteristics observed across the four types of schist. The proposed preventive measures, developed through a systematic analysis of schist disintegration mechanisms, provide an effective framework for slope stability management. This research offers valuable insights into the weathering characteristics of rock masses in slope engineering, which is significant for understanding the progressive failure modes of disintegrating metamorphic formations.

Keywords: slope; schist; thin section identification; mechanism; disintegration resistance test

check for updates

Academic Editors: Qingbang Meng, Raymond Cecil Everson and Blaž Likozar

Received: 24 January 2025
Revised: 24 February 2025
Accepted: 18 March 2025
Published: 20 March 2025

Citation: Wen, Y.; Niu, X.; Lu, Y.; Cheng, Y.; Lu, P.; Xia, J.; Lin, Y.; Tang, L.; Nie, Q.; Lin, K. Study on the Disintegration Resistance of Different Types of Schist on the Eastern Slope of the Tongman Open-Pit Mine. *Processes* **2025**, *13*, 915. https://doi.org/10.3390/pr13030915

Copyright: © 2025 by the authors. Licensee MDPI, Basel, Switzerland. This article is an open access article distributed under the terms and conditions of the Creative Commons Attribution (CC BY) license (https://creativecommons.org/licenses/by/4.0/).

1. Introduction

Schist is commonly found in open-pit mining operations and is highly sensitive to environmental conditions. This sensitivity is characterized by a tendency to soften and disintegrate upon exposure to water or heat [1–3], leading to a reduction in the strength of the rock mass in localized areas of the slope surface. Moreover, the disintegration and failure of schist on the slope generates large amounts of loose materials, which weakens the slope's resistance to erosion. Under the influence of rainfall, this process further exacerbates slope erosion, significantly impacting the overall stability of the slope [4,5].

Therefore, studying the disintegration resistance characteristics and mechanisms of schist is crucial for preventing geological hazards in mining areas and ensuring safety during mining operations.

The existing research on rock disintegration tests primarily focused on macro parameters, such as the cycle number, immersion time, moisture content, and residue mass, to describe the variation patterns during the disintegration process [6–10]. As technology has progressed, numerous scholars have employed techniques, such as X-ray diffraction and Computed Tomography Scans, to analyze the microstructural features of rocks, including the mineral composition, degree of fracture development, cementation, and changes in pore structure, to elucidate the intrinsic factors of rock disintegration [11–14].

In recent years, many achievements regarding rock disintegration models have been established using statistical theories and related concepts [15,16]. Some researchers applied the concept of fractal dimensions from fractal theory to explore the characteristics of rock disintegration. They developed fractal models to study rock disintegration and concluded that the disintegration mechanism involves the initiation and propagation of internal microcracks, as well as the subsequent fragmentation of the rock along these cracks [17–20]. Based on the concept of granular entropy, Zhang et al. [21] pointed out that standard basic entropy is an important indicator for evaluating the disintegration properties of rocks. Liu et al. [22] developed an energy dissipation model for the disintegration of red sandstone based on the principle of energy dissipation.

Numerous researchers have conducted studies on rock disintegration focusing on the characteristics of the rock occurrence environment, including solution environments, temperature variations, and stress conditions [23,24]. Liu et al. [25] indicated that limestone exhibits distinct disintegration characteristics in solutions with varying pH levels, with lower pH values leading to more pronounced changes in the mass fraction of particles of different sizes and more severe disintegration. Zhang et al. [26] conducted laboratory disintegration tests on basalt, considering the effects of climatic factors, and established the relationship between disintegration rates and wet-dry cycles. Zhou et al. [27] explored the mechanical behavior of red soft rock under various water conditions and clarified the changes in the mechanical properties of soft rock under the combined effects of water, stress, and fractures.

Regarding disintegration mechanisms, Yin et al. [28] concluded from their experiments that the disintegration process of red sandstone involves an outward-to-inward interfacial process and damage caused by water absorption and infiltration. Liu et al. [29] found through experiments that the dissolution and differential expansion of clay minerals are the primary factors affecting the disintegration of carbonaceous rocks. Yang et al. [30] proposed that the disintegration of mudstone is primarily influenced by the secondary pores formed during water saturation and the tensile stress exerted on the mudstone surface. The expansion of these pores led to the formation of cracks, and the interconnection of these cracks ultimately caused the disintegration of the sample.

Current research on rock disintegration characteristics primarily focuses on the dissolution environments, structural compositions, and micro-mechanisms of sandstone and mudstone, with limited studies on the disintegration properties of schist. In practical engineering, the material composition of schist may vary across different regions of the same slope. It is crucial to study the disintegration resistance of various types of schist. Therefore, this study focused on four types of schist from the eastern slope of the Tongman open-pit mine. We analyzed the morphological characteristics of the disintegration residues and the variation patterns of the disintegration resistance index for the four types of schist using laboratory disintegration resistance tests and thin section identification. Furthermore, this research examined the disintegration patterns and the mechanisms that account for the

differences in resistance to disintegration among the four types of schist. Finally, preventive measures to mitigate schist disintegration were proposed. This study provides valuable insights into the study of the disintegration characteristics of slope rock mass.

2. Raw Data and Methodology

2.1. Overview of the Study Subject

The eastern slope of the Tongman open-pit mine features a widespread distribution of schist, which mainly includes gray muscovite schist, greenish-gray muscovite schist, gray weakly chloritized biotite–muscovite schist, and greenish-gray chlorite-bearing muscovite schist. The schist, characterized by rapid disintegration and fragmentation upon water exposure, as well as internal structural damage under thermal effects, is highly sensitive to its surrounding environmental conditions. Its poor mechanical properties significantly impact the long-term stability of slopes. To investigate the resistance of the schist to softening and disintegration on the eastern slope of the Tongman open-pit mine, four types of schist samples were collected from different areas of the slope and subjected to laboratory disintegration resistance tests. The distribution areas of the four types of schist on the slope and the planar locations of the sampling points are illustrated in Figure 1.

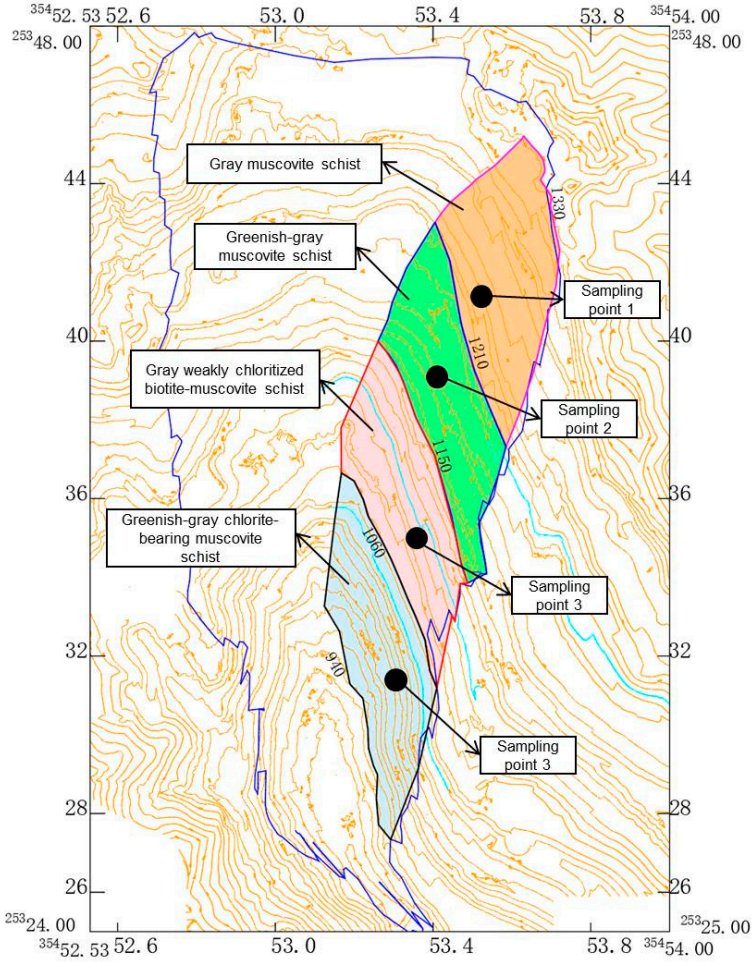


Figure 1. Planar locations of sampling points.

2.2. Thin Section Identification Results of the Four Types of Schist

The four types of schist samples collected from the field were polished into thin sections and examined under a polarizing microscope. The mineral compositions and structural characteristics of the four types of schist are presented in Tables 1 and 2, respectively.

Table 1. Mineral composition of the four types of schist.

Rock Classification	Mineral Composition and Content (%)					
	Muscovite	Quartz	Chlorite	Altered Biotite	Metallic Minerals	Iron-Rich Material
Gray muscovite schist	55	40	3	—	—	2
Greenish-gray muscovite schist	50	40	5	4	1	—
Gray weakly chloritized biotite–muscovite schist	48	39	10	5	1	—
Greenish-gray chlorite-bearing muscovite schist	45	39	15	—	1	—

Table 2. Structural characteristics of the four types of schist.

Rock Classification	Description of Rock Structure Characteristics
Gray muscovite schist	The rock primarily consists of flaky muscovite, granular quartz, chlorite, and iron-rich material. The flaky muscovite and chlorite are oriented in a discontinuous–continuous arrangement, forming a foliated structure. The quartz has been fully recrystallized into anhedral grains, interlocking with one another in straight linear contacts.
Greenish-gray muscovite schist	The rock is primarily composed of platy muscovite, granular quartz, and chlorite. The platy muscovite and chlorite are continuously aligned in a preferred orientation, forming a foliated structure. The quartz has been fully recrystallized into anhedral grains, interlocking with one another.
Gray weakly chloritized biotite–muscovite schist	The rock mainly consists of flaky muscovite with a particle size of 0.05–0.2 mm, granular quartz, and chlorite. The flaky muscovite is continuously oriented, forming a layered structure. The porphyroblasts have been altered into platy biotite grains with a particle size of 0.4–2.5 mm, which are sporadically distributed. Quartz inclusions are commonly present within the biotite grains, and some of the biotite has undergone chloritization.
Greenish-gray chlorite-bearing muscovite schist	The rock is primarily composed of platy muscovite, granular quartz, and chlorite. The platy muscovite is generally arranged in a continuous preferred orientation, forming a foliated structure. The quartz has been fully recrystallized into anhedral grains, interlocking with one another. The chlorite exhibits a discontinuous to continuous preferred orientation.

As revealed in Tables 1 and 2, the main mineral compositions of the four types of schist include biotite and quartz, with the biotite content ranging from 45% to 55% and the quartz content ranging from 39% to 40%. The secondary component is chlorite, with a content of 3% to 15%. In addition, the schist contains altered biotite, metallic minerals, and iron-rich material. Thin-section identification reveals that the internal structure of the schist is heterogeneous and discontinuous, with initial defects of varying scales. The rock matrix exhibits a granoblastic and lepidoblastic texture, where muscovite is continuously aligned to form a foliated structure. The quartz has undergone complete recrystallization into anhedral grains, interlocking with each other in straight linear contacts, while the chlorite is unevenly distributed within the rock.

2.3. Disintegration Resistance Testing Method

To evaluate the schist's resistance to softening and disintegration under high-temperature, humidity, and rainfall conditions, disintegration resistance tests were conducted following a method proposed by Franklin et al. The testing procedure is as follows [31]:

Four groups of schist samples, each weighing approximately 200–300 g, were dried in an oven at a temperature of 105–110 °C until a constant weight was achieved. After cooling to room temperature in a desiccator, the samples were weighed and then immersed freely

in water for 12 h. After the specified duration, the samples were removed and placed into a sieve drum, which was then positioned in the HNB-1 disintegration resistance testing machine for testing. The sieve drum was rotated at a speed of 20 r/min for 10 min, after which the residual samples in the sieve drum were extracted and dried again at 105–110 °C for 12 h. After cooling to room temperature in a desiccator, the samples were weighed again to complete one cycle. The testing process is illustrated in Figure 2.

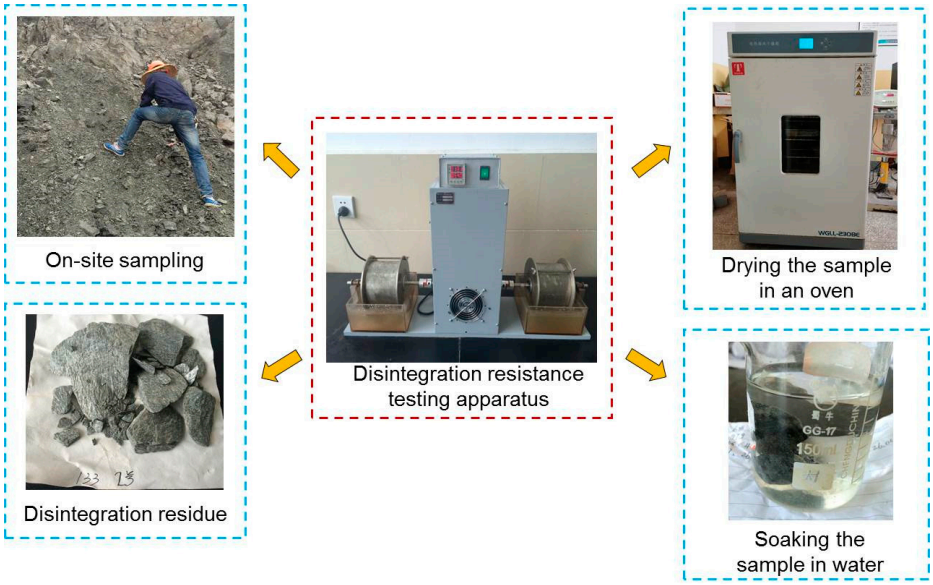


Figure 2. The process for the disintegration resistance testing.

Atmospheric rainfall corresponds to the immersion state in the experiment, while exposure to wind and sunlight represents the drying state. Therefore, the environmental conditions of an open-pit slope can be generalized into these two states, which alternate repeatedly. Consequently, multiple experimental cycles should be conducted during testing, as a single experimental cycle cannot accurately represent the actual disintegration behavior of the slope's surface rock mass. In this study, the number of disintegration resistance cycles was set to 8, and the disintegration resistance index of the schist, I_{dn}, is defined as follows:

$$I_{dn} = \frac{m_n}{m_d} \times 100\% \quad (1)$$

where I_{dn} represents the disintegration resistance index of the rock after n cycles (%); m_d is the dry mass of the original sample (g); and m_n is the dry mass of the residual sample after the nth cycle (g).

3. Results and Discussion

3.1. Morphological Changes of Disintegration Residues of Different Types of Schist

(1) Gray muscovite schist

During the eight-cycle experiment, the gray muscovite schist samples began to disintegrate into thin flaky rock fragments after two cycles. With the accumulation of test cycles, the angular edges of the flaky rock fragments gradually became blunted, and by the later stages, the angular edges had almost disappeared. The disintegration residues were predominantly thin flakes with a thickness ranging from 1 to 5 mm. The morphological changes of the disintegration residues of the gray muscovite schist under different test cycles are displayed in Figure 3.



Figure 3. Morphological changes of disintegration residues of gray muscovite schist under different test cycles: (**a**) Initial rock sample; (**b**) Secondary cycle; (**c**) Fifth cycle; and (**d**) Eighth cycle.

(2) Greenish-gray muscovite schist

During the eight-cycle experiment, the surface of the greenish-gray muscovite schist sample began to locally peel off and disintegrate into small thin flakes along one corner after two cycles. These fragments measured approximately 1–3 cm in diameter and 2–4 mm in thickness. Visible microcracks were observed along the schistosity planes. As the number of test cycles increased, the angular edges of the rock sample gradually became rounded, and the rock disintegrated into fragment-like pieces. The disintegration residues exhibited a medium-thick flaky morphology, with a thickness ranging from approximately 3 mm to 8 mm. The morphological changes of the disintegration residues of the greenish-gray muscovite schist under different test cycles are shown in Figure 4.



Figure 4. Morphological changes of disintegration residues of greenish-gray muscovite schist: (**a**) Initial rock sample; (**b**) Secondary cycle; (**c**) Fifth cycle; and (**d**) Eighth cycle.

(3) Gray weakly chloritized biotite–muscovite schist

During the eight-cycle experiment, the surface of the gray weakly chloritized biotite–muscovite schist sample began to locally disintegrate on one side after two cycles. The disintegration residues appeared in the form of fine strips and granular fragments, with particle sizes ranging from approximately 1 mm to 5 mm. As the number of test cycles increased, the angular edges of both the disintegration residues and the main rock block became rounded. The main rock block remained relatively intact, while the disintegration residues further broke down into fine-grained rock particles. The morphological changes of the disintegration residues of the gray weakly chloritized biotite–muscovite schist under different test cycles are shown in Figure 5.



Figure 5. Morphological changes in disintegration residues of gray weakly chloritized biotite–muscovite schist: (**a**) Initial rock sample; (**b**) Secondary cycle; (**c**) Fifth cycle; and (**d**) Eighth cycle.

(4) Greenish-gray chlorite-bearing muscovite schist

During the experiment, the rock samples of the greenish-gray chlorite-bearing muscovite schist showed minimal disintegration. Instead, the rock blocks spalled off into small fragments, with particle sizes ranging from approximately 1 to 5 mm. The angular edges of the rock blocks became rounded and exhibited a fine-grained texture. The disintegration process and morphological changes of the greenish-gray chlorite-bearing muscovite schist under different test cycles are illustrated in Figure 6.



Figure 6. Morphological changes of residual rock blocks of greenish-gray chlorite-bearing muscovite schist: (**a**) Initial rock sample; (**b**) Secondary cycle; (**c**) Fifth cycle; and (**d**) Eighth cycle.

3.2. Impact of Disintegration Cycles and Mineral Composition on Disintegration Resistance Index

(1) Effect of number of cycles on disintegration resistance index

The results from the disintegration tests of the different types of schist samples are shown in Table 3. The relationship between the disintegration resistance index and the number of cycles across different types of schist samples is illustrated in Figure 7.

Table 3. Disintegration resistance for four types of schist under different cycles.

Rock Classification	Disintegration Resistance Index Under Different Cycles/%							
	1	**2**	**3**	**4**	**5**	**6**	**7**	**8**
Gray muscovite schist	94.65	91.76	88.65	84.12	82.65	80.23	77.39	76.75
Greenish-gray muscovite schist	95.86	93.58	92.68	92.22	90.12	88.26	86.26	86.66
Gray weakly chloritized biotite–muscovite schist	99.12	98.69	98.15	97.57	96.97	96.63	96.13	95.89
Greenish-gray chlorite-bearing muscovite schist	99.85	99.73	99.51	99.33	99.09	98.69	98.39	98.19

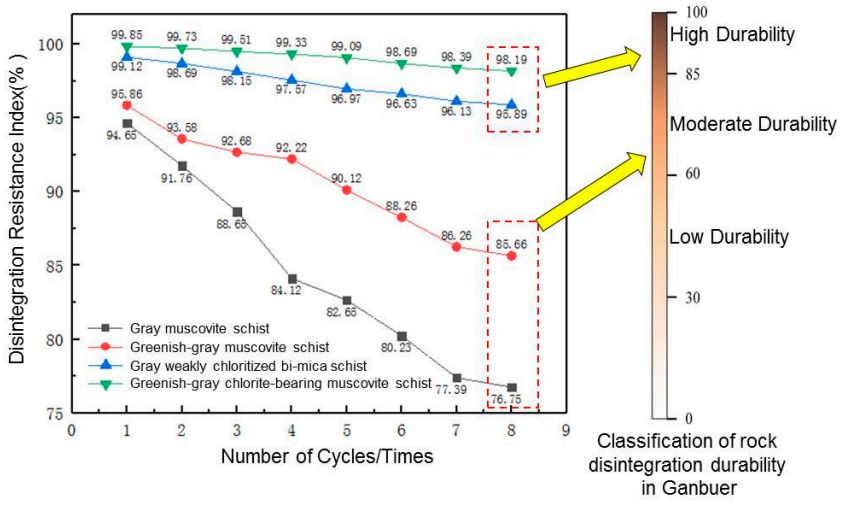


Figure 7. Relationship between the disintegration resistance index and the number of cycles for four types of schist.

Table 3 and Figure 7 revealed that the disintegration resistance indices of the four types of schist decreased with increasing number of cycles, indicating an intensification of disintegration. There were significant differences in disintegration resistance among the different types of schist. For the same number of cycles, the greenish-gray chlorite-bearing muscovite schist exhibited the highest disintegration resistance index at 98.19%, indicating a relatively high degree of rock integrity. In contrast, the gray muscovite schist had the lowest disintegration resistance index at 76.75%, suggesting severe rock fragmentation. The disintegration resistance of the four types of schist was further quantitatively evaluated based on the disintegration resistance index and the Gamble classification of rock durability [32]. The greenish-gray chlorite-bearing muscovite schist and the gray weakly chloritized biotite–muscovite schist are classified as highly durable, while the gray muscovite schist and the greenish-gray muscovite schist are categorized as moderately durable. In addition, rock durability increased as the disintegration resistance index grew.

(2) Variance analysis of disintegration resistance of different types of schist

Based on the experimental results presented in Table 3, a variance analysis was conducted on the disintegration resistance index of the four types of under different numbers of cycles. The results are detailed in Table 4.

Table 4. ANOVA.

Index	Rock Types (Mean ± Standard Deviation)				F	*p*
	Gray Weakly Chloritized Biotite–Muscovite Schist	Gray Muscovite Schist	Greenish-Gray Chlorite-Bearing Muscovite Schist	Greenish-Gray Muscovite Schist		
disintegration resistance index %	97.39 ± 1.19	84.53 ± 6.60	99.10 ± 0.62	90.70 ± 3.45	24.844	0.000 ***

* $p < 0.05$ ** $p < 0.01$ *** $p < 0.001$.

Table 4 demonstrated that the samples from various rock types all *exhibit* significant disintegration resistance indices, which are ranked as follows: greenish-gray chlorite-bearing muscovite schist > gray weakly chloritized biotite–muscovite schist > greenish-gray muscovite schist > gray muscovite schist. There are notable differences in the disintegration resistance among the four types of schist. The main reason for this observation is the variation in the proportion of mineral components within the schist samples. According to the mineral component data in Table 1, muscovite and quartz are the main constituents of the schist. The resistance index of the schist increases as the muscovite content decreases, suggesting that changes in muscovite content have a substantial impact on its disintegration resistance. The quartz content across the four types of schist typically ranges from 39% to 40%, showing minimal variation. Changes in quartz content have a minor effect on the disintegration resistance index.

3.3. Morphological Characteristics of Disintegration Residues and Disintegration Patterns

Morphological analysis was conducted on the disintegration residues presented in Figures 3–6. Based on the morphological characteristics of schist disintegration residues, they were categorized into four patterns. The first pattern: When failure occurred along foliation or bedding planes, the disintegration residues exhibited a thin, flaky shape with a thickness ranging from 5 mm to 10 mm and a length of 10 mm to 30 mm. The second pattern: When failure occurred along foliation or bedding planes, the residues exhibited a moderately thick flaky shape with a thickness of 8 mm to 12 mm and a length of 10 mm to 30 mm. The third pattern: When failure occurred along foliation or bedding planes, the

residues appeared in blocky strips, with a thickness of 5 mm to 20 mm and a particle size of approximately 10 mm to 30 mm. The fourth pattern: When the rock underwent fractured failure, the residues consisted of irregular granular particles with a size ranging from 1 mm to 6 mm. The four morphological patterns of the disintegration residues are illustrated in Figure 8.

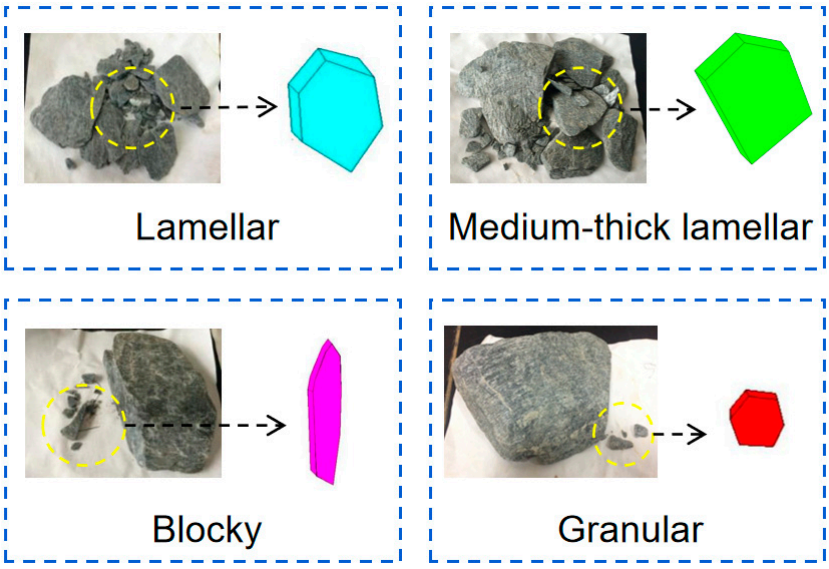


Figure 8. Morphology of disintegration residues.

Based on the observed morphological patterns of the disintegration residues and the schist disintegration process, it can be concluded that the deterioration of schist exhibits significant irregularity. Schematic diagrams of the disintegration and failure patterns for the four types of schist are presented in Figure 9.

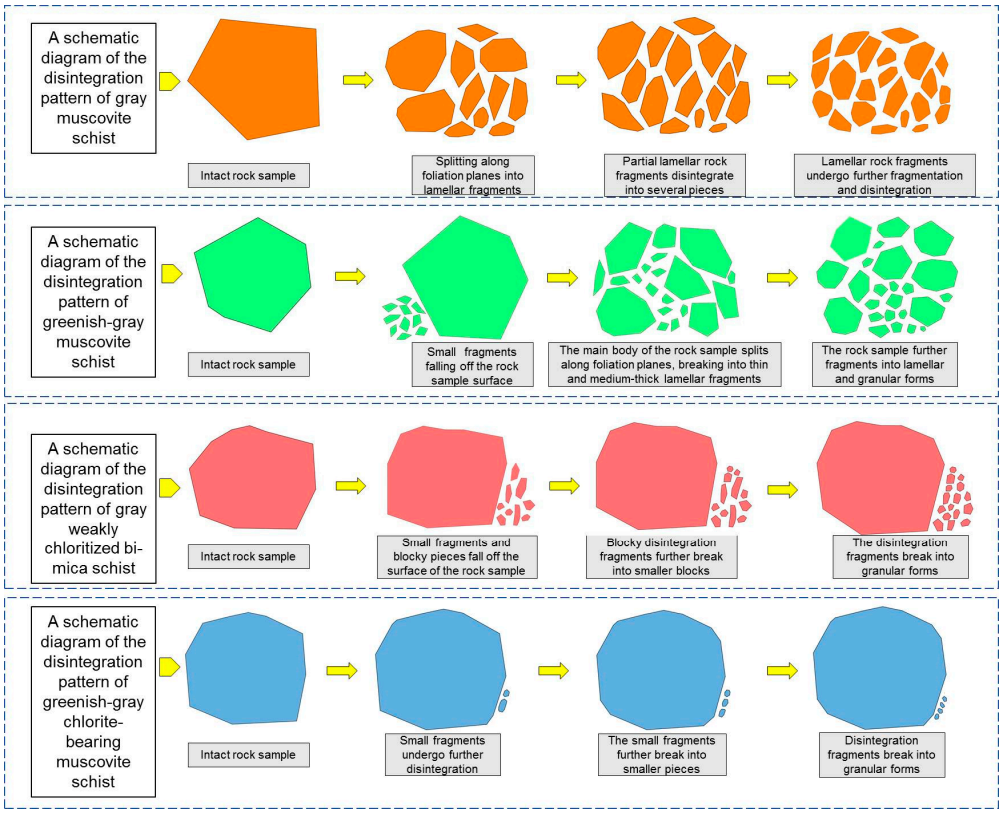


Figure 9. Schematic diagrams of disintegration patterns for four types of schist.

4. Analysis of Microscopic Pore Damage in Schist

Rock disintegration primarily occurs due to the expansion of internal fractures along joint planes. According to the principle of fracture energy consumption, cracks tend to propagate along weak planes [33]. Therefore, the disintegration and failure of schist during the disintegration process develop along the weak planes of foliation. The contact interfaces between flaky muscovite and quartz crystals, which determine pore sizes, provide pathways for the disintegration of schist and determine the resistance of the four types of schist to disintegration and failure.

This study analyzed the mechanisms responsible for the disintegration differences among the four types of schist from a microscopic perspective, based on the pore damage theory. Microscopically, schist is composed of three main components: weak materials, such as muscovite, hard materials, such as quartz and chlorite, and pore defects [34]. The total volume of a rock is the sum of the pore space volume and the solid particle volume. Therefore, the schist can be simplified into a volumetric model, as illustrated in Figure 10.

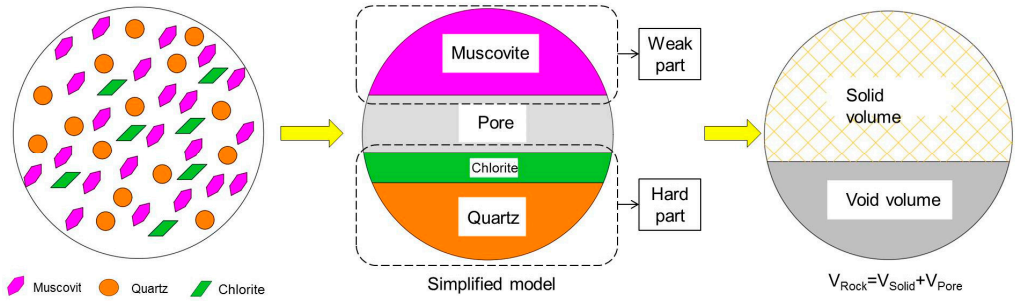


Figure 10. Simplified model for the microstructure of schist.

The porosity of schist is positively correlated with its internal mica mineral content [35]. Based on the muscovite content of the four types of schist shown in Figure 8, the porosity ranks as follows: gray muscovite schist > greenish-gray muscovite schist > gray weakly chloritized biotite–muscovite schist > greenish-gray chlorite-bearing muscovite schist.

Thus, the gray muscovite schist has the smallest solid volume, while the greenish-gray chlorite-bearing muscovite schist has the largest solid volume. Meanwhile, chlorite tends to fill pore spaces; thus, higher chlorite content occupies more pore spaces, resulting in a relatively larger solid volume of the rock. According to the volumetric model, the solid space volume of the four types of schist follows the following relationship:

$$S_1 < S_2 < S_3 < S_4 \tag{2}$$

The volume of pore space is given by the following:

$$P = V - S \tag{3}$$

where S represents the volume of solid space; V denotes the volume of the rock sample; and P refers to the volume of pore space.

The porosity ϕ of the rock sample is defined as follows:

$$\phi = \frac{P}{V} = \frac{V - S}{V} \times 100\% \tag{4}$$

When the volume of the rock sample is constant, it can be determined from Equation (4) that

$$\phi_1 > \phi_2 > \phi_3 > \phi_4 \tag{5}$$

where ϕ_1 represents the porosity of the gray muscovite schist; ϕ_2 represents the porosity of the greenish-gray muscovite schist; ϕ_3 represents the porosity of the gray weakly chloritized biotite–muscovite schist; and ϕ_4 represents the porosity of the greenish-gray chlorite-bearing muscovite schist. The damage constitutive model proposed by Meng [36] is introduced as follows:

$$D_i = \frac{\phi - 0.01}{0.99} \tag{6}$$

where ϕ represents the porosity of the rock at different time points; and D_i is the damage factor with porosity ϕ as the damage variable.

By combining Equations (5) and (6), the ranking of the damage factors for the four types of schist is presented in Equation (7):

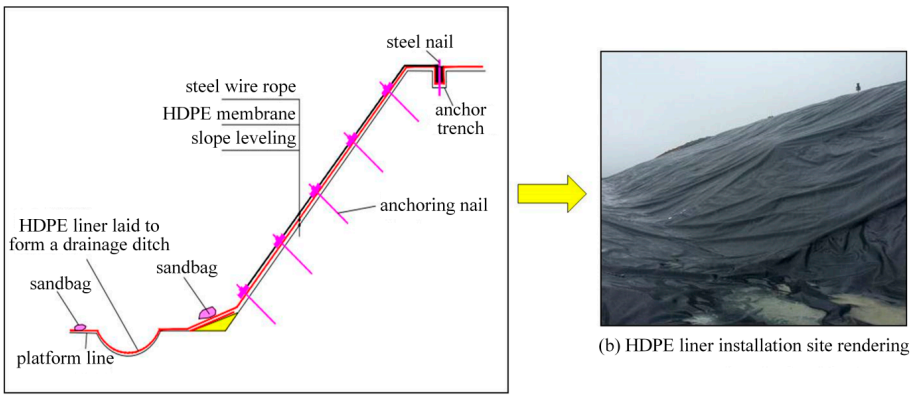
$$D_1 > D_2 > D_3 > D_4 \tag{7}$$

where D_1 represents the damage factor of the gray muscovite schist; D_2 represents the damage factor of the greenish-gray muscovite schist; D_3 represents the damage factor of the gray weakly chloritized biotite–muscovite schist; and D_4 represents the damage factor of the greenish-gray chlorite-bearing muscovite schist.

The above-mentioned analysis of microscopic pore damage in schist indicated that schist with a higher porosity has a larger damage factor, making it more susceptible to weathering and disintegration under changing environmental conditions. Consequently, the four types of schist on the eastern slope of the Tongman open-pit mine exhibited certain differences in disintegration. The initial porosity of schist is determined by the contents of muscovite, quartz, and chlorite, which collectively influence the damage factor of the rock. Therefore, the microscopic damage of the rock is an intrinsic factor affecting its disintegration resistance.

5. Prevention Measures for Schist Disintegration

These findings suggest that schist disintegration is primarily caused by the development of joint fractures in the rock mass due to rainfall. This process leads to micro-damage resulting from pore development, which subsequently reduces the shear strength of the slope rock mass and contributes to slope instability. Therefore, it is essential to adopt measures to prevent seepage on the slope surface. Based on the site conditions, HDPE membranes were installed to prevent weathering and disintegration of the schist on the slope. This flexible material not only provides durable seepage prevention and outstanding effectiveness, but also allows for a straightforward and efficient installation. Once the bench slope is excavated, the material is easy to transfer and reuse, thus significantly reducing construction cost. The installation scheme for the anti-seepage membrane is illustrated in Figure 11.



(a) HDPE liner installation design cross-section diagram

(b) HDPE liner installation site rendering

Figure 11. Anti-seepage membrane scheme.

6. Conclusions

This study focused on the schist on the eastern slope of the Tongman open-pit mine as the research object. The morphological characteristics, disintegration patterns, and variation patterns of the disintegration resistance index across the four types of schist were examined using laboratory disintegration resistance tests and thin section identification. Additionally, the mechanisms responsible for the differences in disintegration among the four types of schist were explored. The following conclusions were obtained:

(1) The disintegration resistance index of the schist was negatively correlated with the number of cycles. Under the same number of cycles, the disintegration resistance indices for the four types of schist were ranked as follows: green-gray chlorite-bearing muscovite schist > gray weakly chloritized biotite–muscovite schist > green-gray muscovite schist > gray muscovite schist.

(2) The analyses of the residues from the disintegration resistance tests identified four morphological patterns of schist disintegration residues: thin sheet-like, moderately thick sheet-like, blocky, and granular.

(3) The microscopic damage analysis revealed that microscopic pore damage in the rock is an intrinsic factor affecting its disintegration resistance.

Author Contributions: Conceptualization, X.N.; methodology, Y.L. (Yongfeng Lu); software, Y.C.; formal analysis, P.L., J.X., Y.L. (You Lin) and L.T.; investigation, Q.N.; data curation, K.L.; writing—original draft preparation, Y.W.; writing—review and editing, Y.L. (Yongfeng Lu). All authors have read and agreed to the published version of the manuscript.

Funding: Yunnan Provincial Science and Technology Department Science and Technology Plan Project: 202401AT070047; Yunnan Provincial Department of Education Fund: 2022J1304.

Data Availability Statement: The original contributions presented in this study are included in the article. Further inquiries can be directed to the corresponding author.

Conflicts of Interest: The authors declare no conflict of interest.

References

1. Zhang, L. Experimental Study on the Slake Durability of Mudstone under the Action of Rainfall and Drying. *Sci. Technol. Eng.* **2020**, *20*, 6221–6227.
2. Tian, W. Experimental study on disintegration characteristics of argillaceous siltstone with different degree of weathering under dry-wet cycling. *J. Water Resour. Water Eng.* **2018**, *29*, 223–226.
3. Zeng, L.; Luo, J.; Hou, P.; Bian, H. Crack Development and Strength Characteristics of Pre-disintegrated Carbonaceous Mudstone Under Dry-wet Cycles. *China J. Highw. Transp.* **2020**, *33*, 1–11.
4. Liu, X.; Zhu, J.; Zeng, P.; Wang, B. Deteriorating Effect of Wetting and Drying Cycles on Bank Slope's Siltstone Properties. *J. Yangtze River Sci. Res. Inst.* **2015**, *32*, 74–77+84.
5. Zhou, Y.; Chen, D.; Yu, J.; Li, Q. Test and Micro-mechanism of Disintegration of Granite Residual Soil under Dry-Wet Cycles. *J. Yangtze River Sci. Res. Inst.* **2023**, *40*, 153–160.
6. Wang, X.; Yao, H.; Dai, L.; Zhang, L.; Lu, J. Experimental Study on Slaking Characteristics of Red-bed Soft Rock in Southern Anhui Province. *Chin. J. Undergr. Space Eng.* **2021**, *17*, 683–691.
7. Yin, S.; Bai, L.; Li, X.; Fu, Y.; Wang, Y. Experimental Study on Disintegration Characteristics of Compacted Granite Residual Soil. *J. Yangtze River Sci. Res. Inst.* **2021**, *38*, 121–127.
8. Liang, B.; Cao, Q.; Wang, J.; Jiang, L. Experimental study on slaking characteristics of feeble disintegration soft rock in drying-wetting cycle. *China Saf. Sci. J.* **2017**, *27*, 91–96.
9. Zhang, D.; Chen, A.; Liu, G. Experimental study on the difference of disintegration characteristics of purple mudstone. *Chin. J. Soil Sci.* **2013**, *44*, 459–464.
10. Li, G.; Wang, J.; Chen, W.; Wu, J.; Cao, X.; Wu, S. Influences of wetting-drying cycles on expansive soils improved with disintegrated sandstone with different particle size groups. *Chin. J. Geotech. Eng.* **2022**, *44*, 643–651.
11. Deng, S.; Li, Y.; Xu, Y.; Wang, N.; Wang, T. Experimental Research on Micro-Failure Mechanism of Watering Disintegration of Red Bed Fine Clastic Rocks. *Saf. Environ. Eng.* **2020**, *27*, 59–66.

12. Guo, Y.; Chen, Q.; Zhou, Z.; Yang, W.-M.; Peng, Z.-H. Quantitative Research and Microcosmic Mechanism Discussion on Red Bed Argillaceous Rock. *Electr. Power Surv. Des.* **2020**, 39–43.
13. Yang, J.; Wang, L.; Li, X.; Li, Y. Micromechanism of disintegration of mudstone in saturation process. *J. Liaoning Tech. Univ. (Nat. Sci.)* **2014**, *33*, 476–480.
14. Liu, X.; Xiong, L.; Luo, W. Micro Characteristics of Disintegration of Red Sandstone of Tongcheng-Pingjiang Expressway. *J. Highw. Transp. Res. Dev.* **2011**, *28*, 7–11.
15. Wang, G.; Yang, S.; Wang, Z. Mechanism analysis and mathematical model study of red sandstone disintegration. *J. Highw. Transp. Res. Dev. (Appl. Technol. Ed.)* **2017**, *13*, 154–156.
16. Wu, X.; Liu, C.; Zhao, K.; Shen, R. Research on Fractal Model of Water-immersed Collapse of Slate. *J. Sichuan Univ. (Eng. Sci. Ed.)* **2008**, *40*, 33–36.
17. Liu, X.; Xu, H.; Zhao, M. Research on Methods of Eliminating the Slacking Properties of Red Beds Soft Rock Based on Fractal Theory. *J. Hunan Univ. (Nat. Sci.)* **2013**, *40*, 27–32.
18. Yang, F.; Zhang, J.; Zheng, C.; Xu, T. Experimental study on disintegration characteristics of red bed soft rock based on fractal principle. *Chin. J. Appl. Mech.* **2022**, *39*, 350–355.
19. Zhao, X.; Li, K.; Xiao, D.; Zeng, C.; Zhang, L. Slaking characteristic of silty mudstone under acid rain action based on fractal dimension. *J. Eng. Geol.* **2020**, *28*, 232–239.
20. Li, Y.; Qi, Y.; Miao, T.; Gao, J. Research on slope alteration sandstone disintegration test and fractal characteristics in open-pit mine. *Opencast Min. Technol.* **2014**, *10*, 15–19.
21. Zhang, Z.; Gao, W.; Tang, X.; Zhang, J.; Han, S. Characteristics of grading entropy of disintegration of swelling rock under dry-wet cycles. *J. Water Resour. Water Eng.* **2019**, *30*, 218–224.
22. Liu, X.; Xiong, L.; Liu, J.; Zhao, M. Slacking mechanism of red sandstone based on energy dissipation principle. *J. Cent. South Univ. (Sci. Technol.)* **2011**, *42*, 3143–3149.
23. Deng, T.; Huang, M.; Zhan, J. Fractal Evolution Law of Clay Rock Disintegration Under Different pH Conditions. *J. Tongji Univ. (Nat. Sci.)* **2014**, *42*, 1480–1485.
24. Zhang, D.; Chen, A.; Su, Y.; Duan, H.; Wang, R.; Liu, G. Effect of hydrothermal environment on disintegration of different purple parent rocks. *Acta Pedol. Sin.* **2013**, *50*, 643–651.
25. Liu, H.; Yao, H.; Cui, Q.; Zhang, Z.; Zhu, D. Experimental analysis of slaking characteristics of rock in different pH solutions. *J. Hefei Univ. Technol. (Nat. Sci.)* **2018**, *41*, 1218–1223+1273.
26. Zhang, X.; Kong, L.; Chen, C.; Yin, S. Experimental investigation on relative contribution of hot and humid weather and heavy rainfall in disintegration of basalt residual soil. *Sci. Sin. (Technol.)* **2016**, *46*, 1175–1184. [CrossRef]
27. Zhou, C.; Su, D.; Qiu, X.; Yang, X.; Liu, Z. Experimental study of cracked soft rock with hydro-mechanical coupling effect. *Acta Sci. Nat. Univ. Sunyatseni* **2019**, *58*, 35–44.
28. Guo, N.; Yang, Y.; Liang, P.; Wang, Z.; Xin, C. Research Progress on Disintegration Mechanism and Reinforcement Method of Sandstone Under Water-Rock Action. *Mater. Rep.* **2023**, *37*, 272–277.
29. Liu, X.; Zhang, T.; Luo, J. Slake Durability and Microstructure Characteristics of Carbonaceous Rocks in Guangxi. *Saf. Environ. Eng.* **2021**, *28*, 41–47.
30. Yang, J.; Wang, L.; Li, X.; Dai, C. Research on disintegration process and micro mechanism of mudstone under water action. *J. Water Resour. Water Eng.* **2014**, *25*, 67–70.
31. *GB/T 50266-2013*; Ministry of Housing and Urban-Rural Development of the People's Republic of China, Standard for Test Methods of Engineering Rock Mass. China Plan Publishing House: Beijing, China, 2013.
32. Huang, S.; Zhou, X.; Zhang, G.; Yao, R.; Liu, M.; Ling, S.; Wu, X. Study on the Disintegration Characteristics and Quantification of Red-bed Soft Rock under the Effect of Dry-wet Cycles in East Sichuan. *J. Railw. Eng. Soc.* **2024**, *41*, 1–6+23.
33. Tang, S.; Huang, R.; Tang, C. Effect of T-stress on crack growth path in rock and fracture strength. *Rock Soil Mech.* **2016**, *37*, 1521–1529+1549.
34. Chen, W.; Zhao, F.; Gong, H. Study of triaxial creep mechanism of mica-quartz schist based on microscopic test. *Chin. J. Rock Mech. Eng.* **2010**, *29*, 3578–3584.
35. Yin, X.; Yan, E.; Wang, L.; Wang, Y. Effect of water and microstructure on wave velocity anisotropy of schist and its mechanism. *Rock Soil Mech.* **2019**, *40*, 2221–2230+2238.
36. Meng, X. Basic Experimental Study on the Damage Evolution Rule of Rock Mass under the Action of Water-Rock. Ph.D. Thesis, Shandong University of Science and Technology, Qingdao, China, 2018.

Disclaimer/Publisher's Note: The statements, opinions and data contained in all publications are solely those of the individual author(s) and contributor(s) and not of MDPI and/or the editor(s). MDPI and/or the editor(s) disclaim responsibility for any injury to people or property resulting from any ideas, methods, instructions or products referred to in the content.